Computers and Electrical Engineering 124 (2025) 110314

Contents lists available at ScienceDirect

Computers and Electrical Engineering

journal homepage: www.elsevier.com/locate/compeleceng

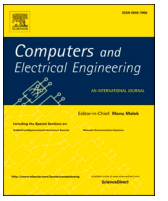

Measurement framework for the consistent and fast measurement of conducted grid emissions in the 9-500 kHz range

Alexander Gallarreta [a,*], Jon González-Ramos [a], Stefano Lodetti [b], Peter Davis [b], Igor Fernández [c], David de la Vega [c], Itziar Angulo [d], Amaia Arrinda [c]

[a] University of the Basque Country (UPV/EHU), Dpt. of Electronic Technology, Donostia-San Sebastián ES- 20018, Spain
[b] National Physical Laboratory (NPL), Teddington TW11 0LW, UK
[c] University of the Basque Country (UPV/EHU), Dpt. of Communications Engineering, Bilbao ES-48013, Spain
[d] University of the Basque Country (UPV/EHU), Dpt. of Applied Mathematics, Bilbao ES-48013, Spain

ARTICLE INFO

Keywords:
Electromagnetic interference
Measurement methods
Power quality
Power line communications
Supraharmonic emissions

ABSTRACT

There is currently no standardized measurement framework for the characterization of conducted emissions in the low-voltage grid for the 9–500 kHz range. Several methods are proposed for the 9–150 kHz band in power quality standards, while the only method defined for the 150–500 kHz range is not designed for power quality measurements. The different configuration of the existing methods prevents consistency of results in the entire band.

This work analyzes drawbacks of the current standardized methods and summarizes the recently published research methods, to propose a measurement framework for the characterization of conducted emissions in the 9–500 kHz range. This framework solves the identified drawbacks by proposing a set of six measurement methods to obtain different metrics for consistent results in the whole range. For that, the use of a common method for obtaining root-mean-square values in the entire 9–500 kHz range is proposed to assess aggregated values and quasi-peak (QP) outputs. Two novel techniques (Approximated-QP and Conservative-QP) are also defined to cover the existing gap in the literature in the estimation of the QP spectra in the 150–500 kHz band. The measurement framework includes a time-frequency domain analysis method to detect and characterize impulsive emissions.

1. Introduction

Over the past decades, multiple policies have been implemented to meet the goal of reducing carbon emissions. These policies, promoted under the Net Zero strategy, have completely changed the concept of the distribution grid, where several energy-efficient devices have been introduced. Moreover, electro-mobility is gaining more and more prominence in the global mobile fleet, in order to reduce the dependence on fossil fuels. As a result, photovoltaic panels (PV), electric vehicle charging stations (EVCSs) and energy storage devices are gaining prominence in the distribution grid, all of them including inverter-based devices, non-linear loads and power electronic devices. Several studies in the last decade have analyzed the impact of these new devices, proving that the power quality (PQ) of the low-voltage (LV) grid can be affected [1], as they generate conducted disturbances in the 2–500 kHz band, also known as 'supraharmonic disturbances', which propagate through the distribution grid. One significant concern is the potential

* Corresponding author at: Dpt. of Electronic Technology, University of the Basque Country (UPV/EHU) ES-48013 Bilbao, Spain.
E-mail address: alexander.gallarreta@ehu.eus (A. Gallarreta).

https://doi.org/10.1016/j.compeleceng.2025.110314
Received 22 January 2024; Received in revised form 15 November 2024; Accepted 30 March 2025
Available online 10 April 2025

interference and disruption in sensitive electronic equipment [2–4], as it is known that the non-intentional emissions may cause thermal stress, audible noise or malfunction in the devices connected to the grid [5]. The conducted disturbances may also interfere the power line communications (PLC) [6–10], which use the distribution grid as propagation channel to transmit information, e.g., energy telemetry data.

Currently, the regulation of conducted emissions in the distribution grid for the 2–500 kHz is still under consideration. Several standardization committees are working on the compilation of the characteristics of interference phenomena (CENELEC TC219 WG11), on the definition of emissions limits in the grid (IEC SC77A WG8) and on the definition of the measurement techniques to assess that phenomenon (IEC SC77A WG9).

The conducted disturbances in the 2–500 kHz band can be grouped in 'intentional' and 'non-intentional' emissions [8]. The intentional emissions are produced intentionally, as a tool to characterize the LV grid or to transmit information via PLC, while non-intentional emissions refer to the spurious disturbances generated by the devices connected to grid. The varied sources of non-intentional emissions generate different time and frequency patterns [8,9,11], which can be classified according to the following types of emissions: impulsive emissions, continuous emissions or varying in amplitude within the fundamental period of grid, if the variation over the time is considered; and narrowband emissions, broadband emissions or colored noise, if spectral characteristics are taken into consideration.

In order to ensure the safe and correct operation of the devices connected to the grid, certain amplitude limits for the conducted disturbances were defined. The IEC 61000–2–2 [12] standard states the maximum amplitude limits for the combination of 'non--intentional' and 'intentional' emissions present in the grid, which are known as compatibility levels (CL). These limits were defined to avoid the interference of 'non-intentional' disturbances on PLC and are intended to be fulfilled in the 95 % of the locations and time. In addition to the CL, several standards have established emission limits for specific equipment. In this context, the EN 50065–1 [13] sets the maximum amplitude levels for PLC transmissions, limiting not only the deliberate emissions injected into the designated transmission channel, but also the unintended out-of-band emissions. Furthermore, the CISPR 14–1:2020 [14], the CISPR 15:2018 [15] and the CISPR 32: 2015 [16] standards define the emission limits for equipment categories such as 'household appliances, electric tools and similar devices', 'multimedia equipment' and 'electrical lighting and related equipment', respectively. However, there are many categories of devices that are not covered by any standard, and as a result, there are no defined emission limits for them. An example is EVCS, for which no specific standards define emission limits, which implies that the only guidance are the CL defined in IEC 61000–2–2.

The measurement techniques to characterize conducted emissions in the LV distribution grid in the 2–500 kHz are linked to a specific frequency sub-range. Hence, different methods are outlined in standards for three frequency ranges (2–9 kHz, 9–150 kHz and 150–500 kHz). Moreover, the standardized methods were developed independently, with different assessment procedures and configuration, preventing from any relation between their results.

Firstly, in the 2–9 kHz range, a unique standardized measurement method is described in the Annex B of IEC 61000–4–7 [17], keeping continuity with the PQ measurement methods below 2 kHz.

Secondly, in the 9–150 kHz band, the 'informative' Annex C of IEC 61000–4–30 Ed.3 [18] standard states that a standard measurement method is under study. In the meantime, it describes three approaches to assess the amplitude of the conducted emissions: the extension of the IEC 61000–4–7 Annex B [17] method up to 150 kHz, the usage of the CISPR 16 [19] receiver and the use of an alternative method with low computational burden that is described in the Annex C of Ed. 3 [18]. Nonetheless, these proposals imply certain issues. To begin with, the annex does not provide information on how to extend the IEC 61000–4–7 Annex B method up to 150 kHz. Regarding the CISPR 16 receivers, the IEC 61000–4–30 Ed.3 standard states that 'the measurement methods in CISPR 16 may be complex or expensive to implement' [18], and moreover, several studies have raised concerns on the usage of this electromagnetic compatibility (EMC) method for grid applications [20]. With respect to the alternative method described in the Annex C of IEC 61000–4–30 Ed.3 [18], this technique is defined to be implemented with measurement gaps, losing the 92 % of the spectral information; additionally, the outputs are not comparable to the previous method since the resolution bandwidth (2 kHz) is one order of magnitude wider.

Thirdly, in the 150–500 kHz range, the PQ standards do not provide guidance on the method that should be used to characterize conducted disturbances in the grid. The unique standardized method for this range, which is defined for EMC compliance but not for PQ measurements, is the CISPR 16 [19] receiver. Above 150 kHz, the configuration of the CISPR method changes in resolution bandwidth, time constants of the detectors and calibration procedure. Therefore, a discontinuity arises in the outputs obtained by the CISPR 16 receiver at 150 kHz, which creates inconsistencies when working with values below and above this frequency threshold. Although CISPR 16 extends this configuration from 150 kHz up to 30 MHz, this work proposes a measurement framework up to 500 kHz, since Narrow-Band PLC technologies use the range up to 500 kHz.

The 9–500 kHz range in the LV grid has gained significant attention in the last years, requiring a consistent measurement strategy due to several reasons. The interference mechanism of conducted emissions exhibits a similar nature throughout the 9–500 kHz range [3,8,9]. In addition, PLC technologies are being deployed in this frequency region, which employ the same configuration in the entire frequency range without differentiating transmission channels below and above 150 kHz [3,8,9]. Furthermore, PLC and PQ related standardization bodies, such as CENELEC TC219 WG11, are showing interest in collecting the interference phenomena occurring in the entire range as a basis for future standardization activities [8].

To address the shortcomings of the standardized measurement methods, and with the aim of covering the existing needs, this contribution proposes a measurement framework based on techniques that are complementary and consistent to characterize the emissions in the 9–500 kHz range. Additionally, this work proposes a simple alternative technique to CISPR 16 for the measurement of quasi-peak (QP) spectra in the 150–500 kHz band.

This paper is organized as follows. Firstly, the state of the art of the measurement framework is presented, where the standardized and research methods are described, and the inconsistencies of the existing measurement methods are pointed out. Secondly, the objectives of the work are described. Thirdly, the approach of the study is defined. Then, the application of the research methods to the 150–500 kHz range is described and analyzed. After that, an empirical relationship between the root-mean-square (RMS) and QP values in the 150–500 kHz is presented, and new alternative methods based on this RMS-QP relationship are proposed and evaluated with grid measurements. To conclude, the complete measurement framework based on complementary techniques for the entire 9–500 kHz band is presented, and the conclusion section summarizes the main outcomes of the study.

2. Objectives

The aim of this work is to define a measurement framework for the consistent characterization of the conducted emissions in the grid from 2 kHz to 500 kHz. This work will compile the existing measurement methods, both standardized and published in the literature, and will analyze the consistency between them in the 2–500 kHz range and with the techniques defined in the PQ standards. In addition, this work analyzes the existing gaps in research and standardized methods with the aim of proposing new techniques to fill these shortcomings up to 500 kHz. Finally, a complete measurement framework is defined to quantify the conducted emissions with the metrics defined in PQ standards (RMS and QP) and to characterize the impulsive emissions separately.

3. Current state of the measurement framework

One of the challenges in dealing with conducted emissions is to obtain suitable accuracy and detailed characterization. For that, specialized measurement equipment and techniques are required to effectively assess the amplitude and variation over time of these disturbances. Currently, there is no standardized measurement framework in the 2–500 kHz band, but a set of measurement methods based on different approaches, configurations and assessment procedures, which generates inconsistencies when comparing results from different methods. To address this issue, several studies have proposed alternative techniques, trying to fill some of the existing gaps, but none of them provides an overall solution nor the necessary procedures to relate results from different assessment methods or to give continuity to results for adjacent frequency ranges. This section describes the standardized techniques and the most relevant published studies for the measurement of conducted emissions for within the 2–500 kHz range, and the inconsistencies to be addressed are identified.

3.1. Standardized measurement methods

The standard measurement techniques for the characterization of the conducted emissions in the 2–500 kHz range are described in the following standards: CISPR 16 [19] standard series, IEC 61000–4–7 [17], and IEC 61000–4–30 [18].

The CISPR receiver [19] was developed to assess the radio interferences between 9 kHz and 400 GHz. The definition of this EMC instrument is based on analogue components and on a black-box approach, where no circuitry is defined, but the performance of the receiver in the form of the expected output values for a set of input signals. This definition generates reproducibility issues, since large tolerances are allowed in the calibration test of the black box approach, which leads to a large number of different possible implementations compliant with the standard [1], but providing different outputs for the same input signals. The most common detector of this technique is the QP detector, which is based on a resistor-capacitor circuit that weights the spectral components, considering not only their amplitude, but also the repetition rate of the emissions. Digital CISPR 16 implementations use shaped windows (Gaussian, Lanczos, kaiser, etc.) with high degree of overlap in the short-time Fourier transform (STFT) to compute the spectral information of the input signals. The Fourier analysis provides spectral outputs every few milliseconds with a resolution bandwidth (RBW) at −6 dB of 200 Hz in the CISPR Band A (9–150 kHz). In the CISPR Band B (0.15–30 MHz), the receiver provides spectral results every tens of microseconds, and the RBW at −6 dB is 9 kHz. The analog behavior of the QP detector can be emulated by infinite impulse response filters or by differential equations, whose charging and discharging performance is defined with time constants provided in the CISPR 16–1–1 standard. Since the digital implementations attempt to simulate the analog behavior of a circuit, the computational burden of a compliant and detailed implementation of this method is very high.

The method described in the Annex B of IEC 61000–4–7 [17] standard was defined to characterize the conducted emissions in the 2–9 kHz band. This method is consistent with the calculation techniques of the traditional harmonic spectrum, which typically ranges from the 2nd to the 40th harmonic of the fundamental frequency. The method applies non-overlapped rectangular windows of 200 ms in the STFT to obtain the spectral information of the signals. The outputs of the spectral analysis, after being grouped to obtain a RBW at −3 dB of 200 Hz, are used to feed different detectors, emphasizing the prevalent application of the RMS detector. Although this method was designed for the 2–9 kHz band, the Annex C of IEC 61000–4–30 Ed.3 [26] suggests its application up to 150 kHz; nevertheless, no guidance on how to extend the method to upper frequencies is provided.

The third method proposed in normative documents is the alternative technique of IEC 61000–4–30 Ed.3 Annex C for the 9–150 kHz range [18]. This method was designed with the purpose of reducing the computational complexity so that it can be implemented in simple and inexpensive devices. It applies a rectangular window of 0.5 ms length in the STFT block, in which only 32 equally spaced time slots of the input signal are used every 10/12 cycles (this is, 200 ms), in order to reduce the computational burden. The outputs of the STFT module have a RBW of 2 kHz, and then, they are used as inputs for the detector stage. The IEC 61000–4–30 Annex C method presents two relevant drawbacks: it loses the 92 % of the measurement content due to the gaps in acquiring the input signal, and the obtained results are not comparable to the previously mentioned methods due to the great difference of the RBW used in this method.

Table 1 summarizes the main characteristics of the measurement methods defined in international standards.

3.2. Research measurement methods

Several research studies have been conducted to propose novel methods to address the drawbacks of the measurement techniques defined in standard documents due to the lack of a standardized measurement framework.

The Subsampling Approach [21] relies on the Nyquist-Shannon sampling theorem to assess the amplitude of the conducted disturbances. This technique, whose main goal is to compute spectral components in inexpensive platforms, implements an analogue filter bank to divide the 9–150 kHz band in 10 sub-bands of 15 kHz bandwidth. Each sub-band is then digitized with a sampling frequency of 30 kS/s, instead of the 300 kS/s that would be necessary to sample the entire band, reducing the required computational burden. The spectral components of each sub-band are then obtained computing STFT with a rectangular window of 0.5 ms.

The estimation by polyphase discrete Fourier transform (DFT) filter bank [22] is a technique that implements a digital filter bank to reduce the sampling frequency of the signal, enabling its implementation in simple devices. In this method the measured signal, which is digitized with a sampling frequency of 1024 kHz, is decomposed into 16 subranges of 32 kHz using the filtering defined in IEC 61000–4–30 [18]. To characterize the 2–150 kHz range, the first 6 sub-ranges are processed with a STFT implementing rectangular windows of 0.5 ms length. The frequency components obtained with this method have an RBW of 2 kHz, as does the alternative method defined in IEC 61000–4–30 Ed. 3 -Annex C [18].

The Wavelet Approach [23] estimates the RMS spectra of the measurements taking advantage of the ‘wavelet package decomposition’. This technique subsequentially filters and downsamples the input signal to 740 frequency bins, with a RBW of 200 Hz, in the 2–150 kHz band. The RMS values of each output filtered signal is then assessed by computing the RMS values over 200 ms intervals.

The matrix pencil method-based [24] approach is a subspace decomposition algorithm to characterize conducted disturbances. The method uses the singular value matrix of signals to assess the frequency components in windows of 0.5 ms. This method estimates the frequency, amplitude, and initial phase of the emissions excluding the interference of the background-colored noise, taking the advantage of the lack of correlation of this noise.

There are a set of measurement methods designed with a common basis, but implementing different approaches for calculating the metrics to quantify the conducted emissions. These methods are the RM-A method [25], the Light-QP method [26], the Statistical-QP method [27] and a technique for the characterization of impulsive emissions [28].

The method providing RMS and Maximum spectra in CISPR Band A (RM-A method) [25] is an adaptation of the IEC 61000–4–7 method for the CISPR Band A (9–150 kHz). The calculation approach of this method ensures the consistency of the spectral components of the PQ techniques for frequencies below and above 9 kHz. The STFT block of this method applies non-overlapped rectangular windows of 20 ms, instead of the 200 ms-length windows defined in IEC 61000–4–7, to obtain the spectral information of the conducted emissions. The output frequency bins are then grouped by applying the ‘symmetrical grouping’ specifically defined for this frequency band, in order to achieve a RBW of 200 Hz and a frequency step size of 100 Hz. The grouped values are then weighted by a set of serial detectors that applies the aggregation intervals defined in PQ standards [18]: 200 ms, 3 s, 10 min. The RM-A method provides results comparable to the IEC 61000–4–7 method in the 9–150 kHz band, but with a higher time resolution of the results, due to the use of the 20 ms length window [25].

The Light-QP [26] is an alternative method to CISPR 16 to provide QP outputs in the 9–150 kHz band. The method relies on the RM-A method to compute the spectral components every 20 ms, and then applies a digital QP detector that weights the RMS values to compute the QP outputs. This method was not designed to fulfill the compliance requirements defined in CISPR 16 standard series, but to provide comparable QP results with lower computational burden.

The Statistical-QP [27] takes advantage of the RM-A to compute the spectral information of the measurements, and then, it applies the conclusions of a statistical analysis that provides an empirical relationship between the RMS and QP values in the 9–150 kHz range for 3 s measurement intervals [27], to estimate QP values. This technique assesses the QP outputs by subtracting to the peak value a quantity proportional to the amplitude fluctuation of the emissions over the measurement time. The Statistical-QP method was not designed to meet the compliance requirements defined in CISPR 16, but to provide comparable QP results for grid measurements in the 9–150 kHz band, as it is described in [27].

The detection and characterization of impulsive disturbances is an aspect not addressed by the standard methods, which only provide information about the emissions in the frequency domain. In [28], a technique for the detection and quantification of the

Table 1
Characteristics of the standardized measurement methods.

Method	Window type	Window length	Window overlap	Meas. gaps	RBW	Frequency-step-size	Detectors/metrics
CISPR 16 (9–150 kHz) [19]	Gaussian, Lanczos, etc.	20 ms	>90 %	No	200 Hz at -6 dB	<100 Hz	Peak, QP, RMS-average, average
CISPR 16 (0.15–30 MHz) [19]		0.5 ms	>90 %	No	9 kHz at-6 dB	<4.5 kHz	
IEC 61000–4–7 – Annex B [17]	Rectang.	200 ms	0 %	No	200 Hz at -3 dB	200 Hz	Peak, RMS
IEC 61000–4–30 – Annex C [18]	Rectang.	0.5 ms	No	Yes	2 kHz at -3 dB	2 kHz	Peak, RMS

impulsive emissions is proposed. This method, which relies also on the RM-A method to obtain the spectra of the measurements, applies a further analysis in the joint time-frequency domain, in order to obtain not only detailed information of the amplitude of the emissions but also the temporal and spectral behavior of them. The impulsive emissions are isolated by selecting the time-spectral components whose amplitude is higher than 10.55 dB with respect to the median value of each frequency bin in 3 s intervals. This amplitude threshold was defined in [28] based on a statistical analysis performed over 15,000,000 time-spectral samples measured in the LV grid. The technique provides not only amplitude information of the impulsive emissions, such as the peak, RMS or minimum values; but also, certain parameters relating the time-behavior of the emissions, including the number of impulsive events, the total duration, the mean duration and the mean duration between impulsive events.

Table 2 summarizes the main characteristics of the measurement methods published in research contributions.

3.3. Inconsistencies in the measurement of conducted emissions

As it is described in the previous section, a wide range of measurement methods is available for the characterization of conducted emissions in the grid for the 2–500 kHz range, but applying different approaches and configurations, and providing outputs with different time and frequency resolutions. Each sub-band in the 2–500 kHz range has different needs, depending on the regulation in force [29] (see Fig. 1).

In the 2–9 kHz band, there is no inconsistencies in the measurement framework from the point of view of conducted emissions. This band is covered by PQ standards, and the IEC 61000–4–7 Annex B [17] document defines the technique to quantify the conducted emissions in the grid.

By contrast, in the 9–150 kHz range, there is a lack of normative directives. As described above, three measurement approaches are proposed in Annex C of IEC 61000–4–30 Ed.3 [18]; nonetheless, this annex is 'informative' and its application is not mandatory. Several studies have been conducted to address the drawbacks present in this frequency range, and a wide set of research measurement methods are available.

The situation in the 150–500 kHz range is completely different, neither the PQ standards nor research contribution have addressed the measurement of conducted emissions in this band. The only method defined for this frequency range, which is not optimized for grid measurements, is the method described in the CISPR 16 series [19]. In addition to the drawbacks that this method presents in the 9–150 kHz band, the method defines different configurations below and above 150 kHz. In particular, for the QP detector applied above 150 kHz, the CISPR 16 defines a wider RBW for the frequency analysis (9 kHz instead of 200 Hz) and different time constants, which leads to relevant discontinuities in the results of this method, when it is applied for the range 9–500 kHz (see Fig. 2). Fig. 2 illustrates the spectral outcomes obtained with a digital CISPR 16 receiver in the 9–500 kHz range for a recording taken in the LV distribution grid, where PLC frames were transmitted. The frequency domain results presented in this plot demonstrate that the CISPR receiver is capable of more precise characterization of conducted emissions in the 9–150 kHz band, due to the RBW of 200 Hz. In the 150–500 kHz range, however, the 9 kHz configuration of the RBW impedes the correct identification of the waveforms present in the LV grid (see Fig. 2). Furthermore, the results below and above 150 kHz cannot be compared due to the differences in the definition of the RBW (see Fig. 2). Nevertheless, as several standards, such as EN 50065–1 [13], CISPR 14–1:2020 [14], CISPR 15:2018 [15] and CISPR 32: 2015 [16], have defined limits in the form of QP values for the 150–500 kHz range, there is a need to develop methods adapted to grid measurements for the calculation of QP values in the 150–500 kHz range.

In summary, the normative methods do not cover in a complete and consistent way the measurements of conducted emissions in the 9–500 kHz range. Moreover, results provided by different standard methods are not comparable and results of the same method show relevant discontinuities over the frequency, due to changes in the assessment configuration. These important inconsistences show the need of defining a measurement framework for the whole frequency range that solves these issues.

Table 2
Characteristics of the measurement methods published in research publications.

Method	Window type	Window length	Window overlap	Meas. gaps	RBW	Frequency-step-size	Detectors/metrics
Subsampling Approach [21]	Rectang.	5 ms	No	Yes	200 Hz at -3 dB	200 Hz	Peak, RMS
Estimation polyphase DFT filter bank [22]	Rectang.	0.5 ms	0 %	No	2 kHz at -3 dB	2 kHz	Peak, RMS
Wavelet Approach [23]	Rectang.	200 ms	0 %	No	200 Hz at -3 dB	200 Hz	Peak, RMS
Matrix pencil method-based approach [24]	Rectang.	0.5 ms	No	No	200 Hz at −3 dB	Non constant	Peak RMS
RM-A method [25]	Rectang.	20 ms	0 %	No	200 Hz at -3 dB	100 Hz	Peak, RMS
Light-QP method [26]	Rectang.	20 ms	0 %	No	200 Hz at -3 dB	100 Hz	QP
Statistical-QP [27]	Rectang.	20 ms	0 %	No	200 Hz at -3 dB	100 Hz	QP
Charact. impulsive emissions in the joint t-f domain [28]	Rectang.	20 ms	0 %	No	200 Hz at -3 dB	100 Hz	Peak, RMS, num. events, mean duration, etc.

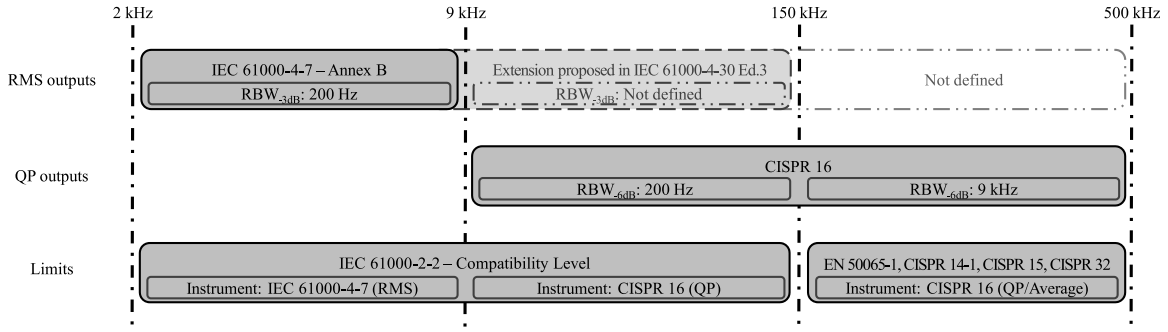

Fig. 1. Overview of the standardized requirements for the measurement of grid conducted emissions.

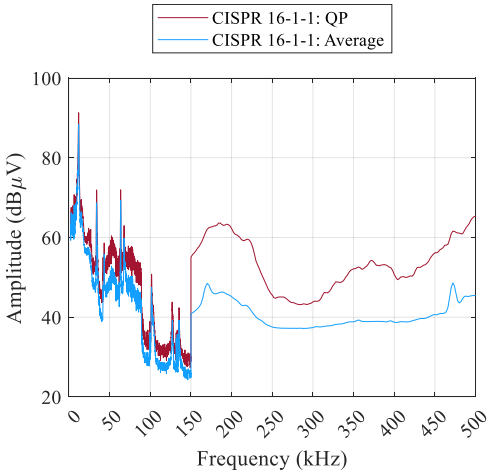

Fig. 2. Outputs of a LV grid measurement, computed in accordance with the configurations outlined by CISPR 16 for Band A (9–150 kHz) and Band B (0.15–30 MHz).

None of the research methods described in Section 3.2 solves the need of providing a complete measurement framework for the entire 9–500 kHz range, as all of them address only one specific need in part of the frequency range, and others do not provide continuity nor consistency with the standard methods for frequencies below 9 kHz.

The most relevant proposal to be considered in the definition of a novel measurement framework is the use of the RM-A method as the basis, since it is consistent with the measurement techniques defined below 9 kHz, and it gives continuity to the results below and above 9 kHz. Nevertheless, this method does not cover the entire 9–500 kHz range, and therefore, the consistency in results above and below 150 kHz is not fulfilled.

Additionally, the relationship between RMS and QP values has been published only for the 9–150 kHz band [27]. The technique to characterize impulsive emissions in the joint time-frequency domain proposed in [28] is also defined only for the 9–150 kHz band [28].

Therefore, the main issues that a complete and consistent measurement framework should address are the following:

- There is no method to provide consistent RMS values for the entire frequency range 9–500 kHz.
- No RMS-QP relationship has been defined for the 150–500 kHz range, and therefore, no method consistent with PQ measurements for the estimation of QP values is available in this frequency range.
- No method has been defined to characterize impulsive emissions in the joint time-frequency domain in the 150–500 kHz range.

4. Approach of the study

This work defines a novel measurement framework with the aim of addressing the gaps identified in the previous section, to establish a consistent characterization procedure of the conducted emissions in the grid for the 9–500 kHz range. The proposed measurement framework must be consistent with the consolidated standard methods and metrics for frequencies below 9 kHz.

The key aspect to ensure a consistent measurement framework is to provide comparable results in the entire band. The main argument for this consistency in the results is to be able to compare the emissions in the whole band and to be able to know their relevance. As the RM-A method is consistent with the measurement techniques defined below 9 kHz, and it gives continuity to the results below and above 9 kHz, this method is selected as a basis for the novel measurement framework up to 500 kHz (see Fig. 3).

The methods Light-QP and Statistical-QP provide QP outputs for the 9–150 kHz, which are consistent to the approach of RM-A method. Therefore, they are good candidates to be part of the measurement framework (see Fig. 3).

The measurement method to characterize impulsive emissions in the joint time-frequency domain for 9–150 kHz is also consistent to the assessment procedure and configurations of the RM-A method. For this reason, it is also selected as a candidate method (see Fig. 3).

Considering all these candidate methods as a basis for the measurement framework for 9–500 kHz, there is still a list of relevant aspects still to be solved (see Fig. 3):

- In order to ensure the consistency with the methods defined below 150 kHz, an extension of the RM-A method is proposed up to 500 kHz. Furthermore, an adaptation of the RM-A method to the 150–500 kHz range is also presented in this paper to obtain spectral values with a RBW similar to the outputs of CISPR 16 (9 kHz) in this range.
- An empirical relationship between RMS and QP spectra is defined in this work for the 150–500 kHz range.
- To estimate QP values in the 150–500 kHz range, two methods (Approximated-QP and Conservative-QP) are defined, using the RMS-QP relationship as a basis.
- In addition, the characterization of impulsive emissions in the joint time-frequency domain for the 150–500 kHz range is also addressed in this paper.

The aspects to be solved are dealt with in the following sections. Firstly, Section 5 contains the assessment of the RMS values up to 500 kHz. Secondly, the characterization of impulsive emissions in the joint time-frequency domain in the 150–500 kHz range is described in Section 6. Thirdly, Section 7 contains the results of the empirical relationship between RMS and QP values for the 150–500 kHz range obtained empirically for the LV distribution grid. Afterwards, the Approximated-QP and Conservative-QP methods, which are based on the empirical RMS-QP relationship, are defined in Section 8. Finally, Section 9 contains the description of the novel measurement framework of this contribution.

The measurement framework presented in this paper addresses the following inconsistencies of the current measurement framework:

- The lack of consistency between results obtained below and above 150 kHz due to the configuration of the measurement methods.
- The lack of PQ measurement methods that provide QP and RMS values in the 150–500 kHz range.
- The lack of RMS-QP relationship in the 150–500 kHz range.
- The lack of technique(s) to characterize the impulsive emissions in the joint time-frequency domain for the 150–500 kHz range.
- Ensure the consistency with the techniques defined for the assessment of conducted disturbances below 9 kHz.

5. Assessment of consistent RMS values up to 500 kHz

This section proposes an extension of the RM-A method [25] up to 500 kHz to compute the RMS values of the conducted emissions. In addition, an adaptation of the RM-A method is also defined for the 150–500 kHz in order to adapt the outputs to the RBW defined for this frequency range (RBW of 9 kHz, in contrast to 200 Hz RBW below 150 kHz).

5.1. Extension of the RM-A method up to 500 kHz to assess RMS values

The approach to extend the RM-A method up to 500 kHz consists of applying the configuration defined in [25] for frequencies below 150 kHz over the entire frequency range. With this approach, it is possible to obtain spectral content with similar characteristics over the entire frequency range: a RBW of 200 Hz and a frequency-step-size of 100 Hz every 20 ms. In addition, these values can be aggregated in the PQ aggregation intervals (200 ms, 3 s, 10 min, etc. according to [18]) to obtain the effective value of the emissions. As a result, the RMS values obtained with the RM-A method, in the original (9–150 kHz) and the extended (150–500 kHz) bands, are consistent over the entire frequency range.

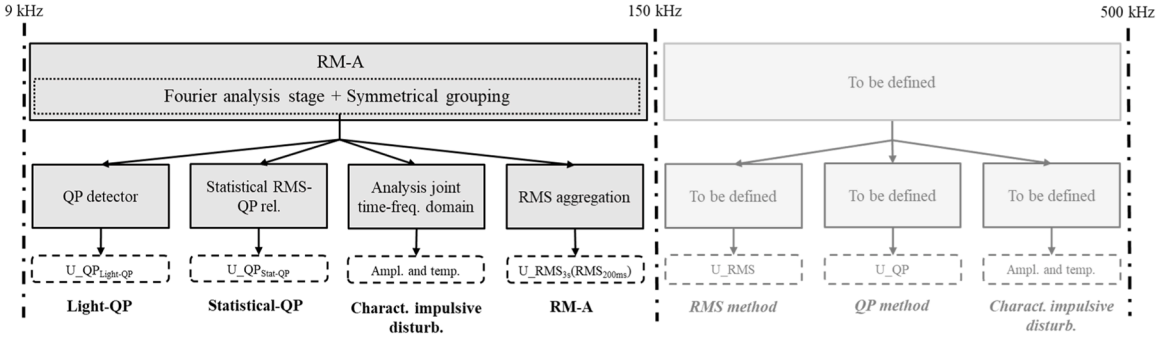

Fig. 3. Schematic overview of the selected research measurement methods and the existing gaps in the 9–500 kHz range.

5.2. Adaptation of the RM-A method to the requirements of QP assessment in the 150-500 kHz range

This section suggests modifying the RM-A method to align with the spectral characteristics outlined in the CISPR 16 method for CISPR Band B (0.15–30 MHz). This involves employing a RBW of 9 kHz and a frequency-step-size of 2 kHz. Once the spectral characteristics are harmonized, the RMS values can be processed using the RMS-QP relationship to derive the desired QP values.

Fig. 4 depicts the sequence of steps involved in adapting the RM-A method to the 150–500 kHz band.

Firstly, the input signal is high-pass filtered by using a 6th order elliptic infinite impulse response filter, whose passband frequency is 150 kHz, the stopband frequency is 147 kHz, the passband ripple is of 0.05 dB and the stopband attenuation is set to 60 dB.

Secondly, the RM-A method ([25]) is applied up to 500 kHz to obtain instantaneous RMS outputs ($Y'_{B,b}$ in Fig. 4) with a RBW of 200 Hz and a frequency-step-size of 100 Hz. The spectral values are then grouped to obtain a RBW of 9 kHz and a frequency-step-size of 2 kHz ($Y'_{D,b}$ in Fig. 4 and Eq. (1)). The RMS values obtained with the RM-A value are then grouped every 2 kHz with the following equation:

$$Y'_{D,b} = \sqrt{\sum_{f=b-4.5\ kHz}^{b+4.5\ kHz} {Y'_{B,f}}^2 \cdot {M_{f-b}}^2} \tag{1}$$

where, $Y'_{D,b}$ are the grouped values with a RBW of 9 kHz and a frequency-step-size of 2 kHz, b is the discrete frequency defined for the 150–500 kHz range with a frequency-step-size of 2 kHz, $Y'_{B,b}$ are the output values of the RM-A method and M_f is the grouping factor. The last parameter, the grouping factor, is used to weight the RMS outputs, it is based on a Gaussian function (see Eq. (2)) and, as shown in Fig. 5, aims to achieve the spectral selectivity determined by CISPR 16 for Band B (0.15–30 MHz):

$$M_f = e^{-\frac{1}{2}\left(\frac{\alpha \cdot f}{(L-1)/2}\right)^2} \quad \forall f \in [-4.5\,kHz, 4.5\,kHz] \tag{2}$$

where M_f is the grouping factor, f is the discrete frequency defined between ±4.5 kHz every 100 Hz, α is the spread parameter being equal to 11.75 and L is 91, which corresponds to the number of elements of the parameter f.

At this stage, using the grouped values ($Y'_{D,b}$) it is possible to extract the maximum value of the emissions in the spectrum by assessing the peak amplitude of each frequency. As shown in Fig. 4, these aggregated values should be calculated over the aggregation interval (200 ms, 3 s, etc.) defined in PQ standards [18]. The aggregated values are used in this paper for further calculation in order to define the RMS-QP relationship for the 150–500 kHz.

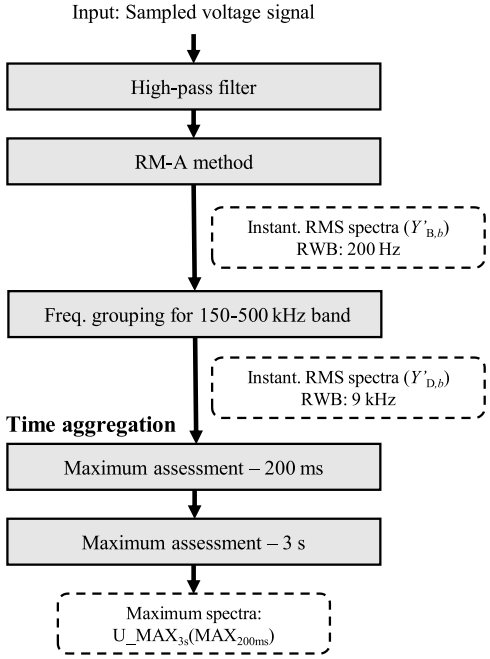

Fig. 4. Schematic overview of the adaptation of the RM-A method to the 150–500 kHz range, to provide: (first) RMS values with continuity for frequencies below 150 kHz; (second) RMS values with the configuration required by the CISPR 16 method for CISPR Band B (0.15–30 MHz) for QP values; (third) MAX values as an intermediate value for QP assessment.

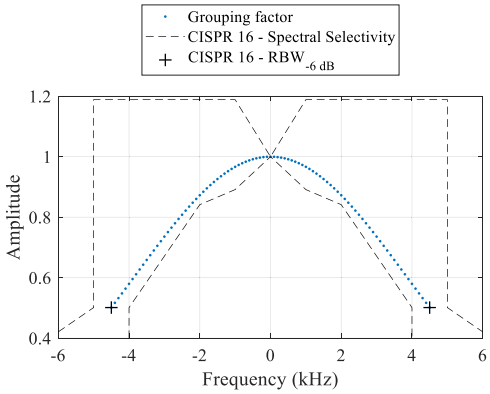

Fig. 5. Spectral selectivity of CISPR 16 for 0.15–30 MHz band and the grouping factor for RM-A outputs.

6. Characterization of impulsive emissions in the joint time-frequency domain for the 150–500 kHz range

The characterization of impulsive emissions in the joint time-frequency domain is an aspect already addressed in [28]. Nevertheless, this contribution is limited to the 9–150 kHz band. This section demonstrates that the methodology used for the detection and characterization of the impulsive emissions can be extended to the 150–500 kHz range.

The input data to this technique is the instantaneous RMS spectra computed by the RM-A method. Then, the median value of the instantaneous RMS spectra over 3 s length intervals is calculated. Then, a threshold of 10.55 dB above the median values of each frequency bin is applied to identify the impulsive emissions that are present at each frequency bin. To demonstrate that the same threshold remains valid in the 150–500 kHz range, a set of grid recordings taken in the LV is used a as a validation. The selected recordings were taken in an urban scenario of the LV distribution grid with the presence of PLC transmissions. The recordings were taken at the point-of-connection (POC) of smart meters implementing PLC technologies to transmit telemetry data. The POCs were located a few hundred meters from the transformers; therefore, the conducted emissions measured in these recordings are mainly generated by the equipment connected to the households and the smart meters. Two representative examples of these recordings are described below.

Fig. 6 (left plot) presents the temporal-spectral information, represented as a spectrogram, of one of the recordings acquired in the LV grid for the 150–500 kHz range. This recording contains three broadband impulsive emissions, indicated with white ovals. The results of applying the extension of the proposed method are shown in the right plot in Fig. 6, where the impulsive emissions have been identified and represented with different colors (depending on their amplitude), while the rest of (non-impulsive) emissions are shown in dark blue. It can be seen that the broadband impulsive emissions are correctly identified also in this frequency range (see Fig. 6, right plot).

Left graph in Fig. 7 contains the spectrogram of another recording taken in the LV grid. This recording also contains broadband impulsive emissions, indicated with a white oval in Fig. 7 (left plot). The right graph in Fig. 7 shows the results of applying the extension of the method to identify the impulsive waveforms of the recording. As it can be seen, the impulsive emissions are clearly

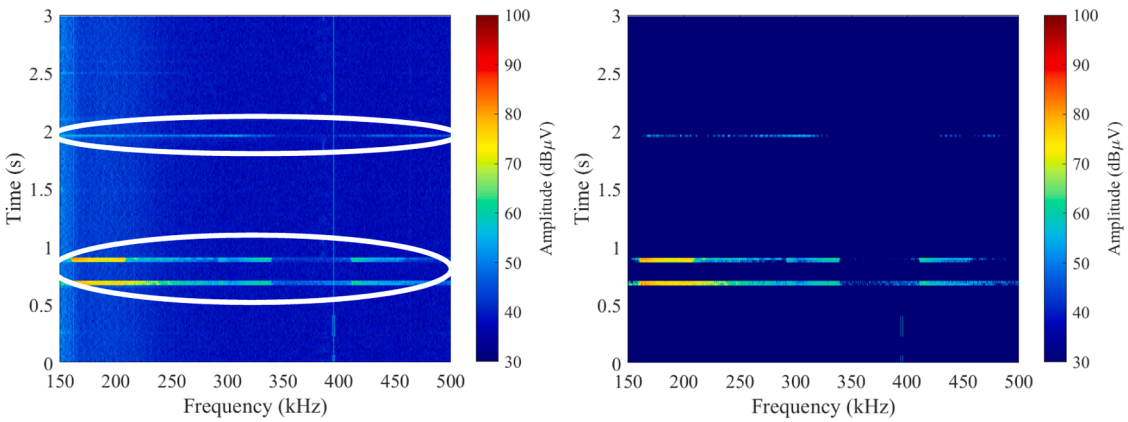

Fig. 6. Left: Spectrogram of a recording measured in the LV grid and processed with the extension of the RM-A method. The recording contains emissions continuous over the time (vertical lines) and impulsive emissions (horizontal lines) in the form of wideband emissions of a few milliseconds. Right: Results of the extension of the joint time-frequency domain method to the 150–500 kHz range to identify impulsive emissions for the waveform.

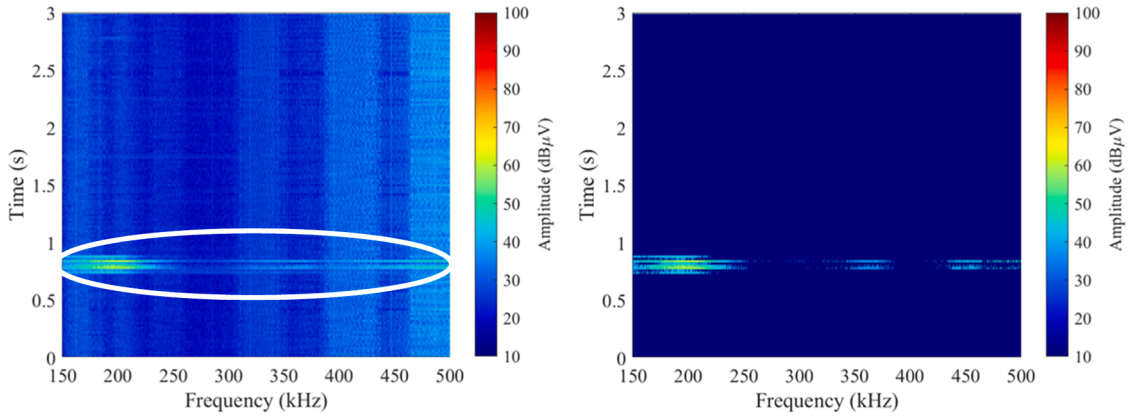

Fig. 7. Left: Spectrogram of another recording measured in the LV grid. Right: Results of the extension of the joint time-frequency domain method to the 150–500 kHz range to identify impulsive emissions for the waveform.

detected.

The results show that the detection technique defined in [28] for the 9–150 kHz band is applicable also to the identification of the impulsive waveforms in 150–500 kHz range. Consequently, this technique is proposed to be included in the measurement framework for the identification and characterization of impulsive emissions in the 9–500 kHz frequency range.

7. Empirical RMS-QP relationship for the 150–500 kHz range

As it has been mentioned in the objectives of the study, and justified in the state of the art, a relationship between RMS and QP spectral values for the conducted emissions in the grid must be defined for the 150–500 kHz band. This section describes the methodology and the results for the definition of an empirical relationship between RMS-QP values in the 150–500 kHz range.

7.1. Input signals

The empirical relationship between the RMS and QP spectra in the 150–500 kHz band has been defined empirically from a dataset of 111 recordings of 3-s length taken in the LV distribution grid. The recordings were taken in several measurement campaigns in Spain and Switzerland: 31 recordings were taken at the POC of EVCS or PV inverters, 48 recordings at points of LV distribution grids with smart meters transmitting information via PLC technologies, and 32 recordings at points of LV grids without PLC transmissions. The recordings were randomly distributed into two groups, one of them (composed of 47 recordings) to define the RMS-QP relationship,

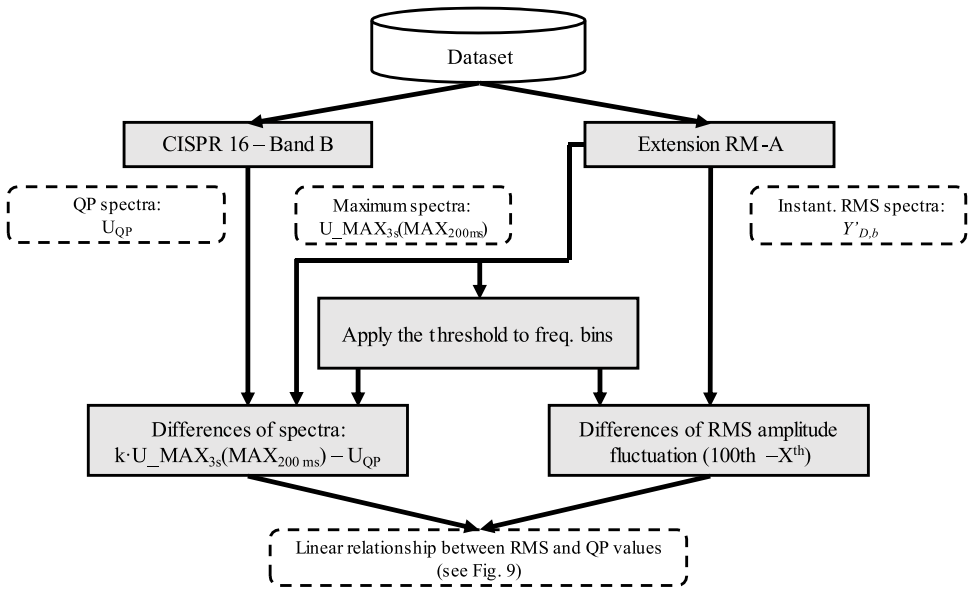

Fig. 8. Overview of the procedure to obtain the relationship between RMS and QP values.

and the second dataset (64 recordings) to validate the outcomes of the study.

All the recordings were recorded with the same measurement set-up [30], which relies on a voltage probe, a digital oscilloscope and a laptop. The voltage probe includes an analog band-pass filter for the 2–500 kHz range and galvanic isolation, to get rid of the fundamental frequency and the leakage generated by harmonic distortions below 2 kHz and to protect the equipment from overvoltage events, respectively [30]. The oscilloscope digitizes the signal filtered by the probe using a 16 bits amplitude resolution and a sampling frequency of 8.92 MS/s, in order to avoid the aliasing that could be generated by the broadcast services. Finally, the sampled signal is sent to the laptop via USB to store the raw data and process the spectra of the recordings.

7.2. Empirical relationship

The empirical relationship between the RMS spectra provided by the extension of the RM-A method and the QP outputs of CISPR 16 has been found by considering the aspects that both metrics represent and a statistical analysis. On one side, the QP detector weights the spectral components taking into account not only the amplitude of the emissions, but also their repetition rate. On the other side, the RMS values obtained during the Fourier analysis of the RM-A method are linked to the mean value of the signal energy, and they are not affected by the repetition rate of the emissions, since only the amplitude is considered. Accordingly, the relationship between RMS and QP values has been found in this study by comparing the difference between the RMS and the QP values with the amplitude fluctuation of the emissions, which is calculated statistically by a combination of percentiles. Fig. 8 presents the flow chart of the procedure to obtain the empirical RMS-QP relationship. The parameters used in the statistical analysis are the following:

- U_{QP}: QP values obtained using a digital implementation of CISPR 16 with Band B (0.15–30 MHz) configuration [19].
- $U\_MAX_{3s}(MAX_{200ms})$: maximum values obtained with the extension of the RM-A method, after the grouping for the 150–500 kHz range, in 3 s measurement intervals.
- $Y'_{D,b}$: instantaneous RMS values obtained every 20 ms with the extension of the RM-A method after the grouping for the 150–500 kHz range.
- k: factor to obtain a proportional value to $U\_MAX_{3s}(MAX_{200ms})$ which is a variable parameter to be optimized during the definition of the empirical relationship.
- X^{th}: parameter in the combination of percentiles (100th-X^{th}) that assesses the amplitude fluctuation of the spectral components, to be optimized on the definition of the empirical relationship.

In this study, 47 grid recordings are used to define the empirical RMS-QP relationship. For each 3-s length measurement interval 26,400 spectral values are obtained, corresponding to the 176 frequency bands in the 150–500 kHz range, whose RBW is of 9 kHz and the frequency-step-size of 2 kHz, and 150 measurement outputs provided by the RM-A method each 20 ms. Therefore, in the definition of the RMS-QP relationship, a total of 1,240,800 spectral values are considered.

7.3. Threshold for the empirical relationship

The background noise is the lowest amplitude emission with random amplitude variability, showing similar RMS and QP amplitude values. For his reason, these very low amplitude emissions have not been included in the statistical analysis, by applying a threshold level to filter out the emissions with lower amplitude. The threshold level is defined as the 50 % of the out of band limits for PLC transmissions defined in the EN 50065–1 for QP measurements in 500 kHz. The emission limit for 500 kHz is 56 dBμV and the threshold level selected in this study is 0.315 mV (see Eq. (3)).

$$Threshold = 50\% \cdot 10^{56/20} = 50\% \cdot 0.631\,mV = 0.315\,mV \tag{3}$$

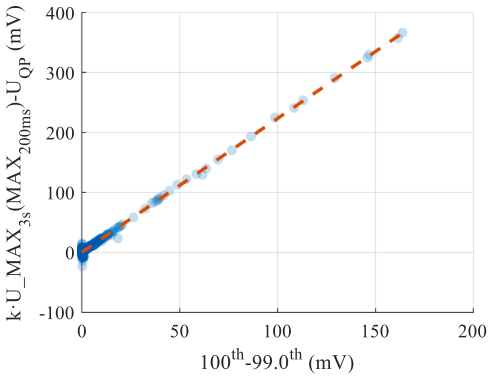

Fig. 9. Example with the 100th-99th percentile combination of the linear relationship between waveforms amplitude variability over the time and the RMS and QP values in the 150–500 kHz band.

7.4. Linear relationship between waveforms amplitude variability over time, RMS and QP values

By applying the procedure described in Fig. 8, a linear relationship can be identified between the following quantities:

- the difference between the maximum spectra obtained with the extension of the RM-A method and the corresponding QP values obtained with CISPR 16 ($k{\cdot}U\_MAX_{3s}(MAX_{200ms})$- U_{QP} in Fig. 8).
- the combination of two percentiles ($100th$-X^{th}) calculated for each frequency component ($Y'_{D,b}$) along the measurement interval of 3 s. The subtraction of a specific percentile to 100th models the amplitude fluctuation of the emissions over the time.

Fig. 9 shows the linear relationship that has been observed for the *100th-99th* combination of percentiles, considering k equal to 3.10. In this graph, the blue dots represent each spectral frequency component, while the orange dashed line is the linear regression line of the displayed data. As observed in Fig. 9, there is a clear correlation between the proportional differences of amplitude of both methods and the combination of percentiles. The linear regression covers not only the trend of the values closer to the origin, but also the more extreme cases.

7.5. Obtaining the numerical RMS-QP relationship

The RMS-QP relationship depends on two parameters: the factor k, to obtain the proportional amplitude value of the U_MAX_{3s}(-MAX_{200ms}), and the parameter X^{th} in the combination of percentiles, to characterize the amplitude variability of the spectral components over the time. The values of both parameters have been obtained computing 126 different configurations, using 6 combination of percentiles and 21 values for k, and optimizing the variables based on the goodness of fit of the trend lines with respect to the data. In addition, in this study 156,340,800 samples have been analyzed during the statistical parametrization of the RMS-QP relationship. Regarding the calculation process of the goodness of fit, it has been assessed computing the root-mean-square-error (RMSE) of the trend lines for the 126 different configurations. The procedure to calculate the RMSE values is the following, where $Trendline_i$ represents the values of the trendline, $data_i$ the real values measured in the LV grid, and N the total number of spectral data used in the definition of the tendency line:

$$RMSE = \sqrt{\frac{\sum_{i=1}^{N}(Trendline_i - data_i)^2}{N}} \tag{4}$$

For the 126 combination of parameters a tendency line has been calculated, which is the basis to define a conversion factor between the RMS and QP spectra. The conversion factor is defined in Eq. (5), relating the combination of percentiles and the difference of the RMS and QP spectra. The conversion factor is defined by the slope of the tendency line, parameter a in Eq. (5), and the y-intercept of the same trendline, which corresponds to parameter b in Eq. (5).

$$Conversion\,factor = \left(100^{th} - X^{th}\right) \cdot a + b \approx k \cdot U\_MAX_{3s}(RMS_{200ms}) - U_{QP} \tag{5}$$

a (mV)

k	100th-99.0th	100th-98.0th	100th-97.0th	100th-96.0th	100th-95.0th	100th-94.0th
2.50	1.633	1.632	1.632	1.631	1.630	1.630
2.55	1.683	1.682	1.681	1.681	1.680	1.680
2.60	1.733	1.732	1.731	1.731	1.730	1.730
2.65	1.782	1.782	1.781	1.781	1.780	1.780
2.70	1.832	1.832	1.831	1.830	1.830	1.830
2.75	1.882	1.881	1.881	1.880	1.880	1.879
2.80	1.932	1.931	1.931	1.930	1.930	1.929
2.85	1.982	1.981	1.980	1.980	1.980	1.979
2.90	2.031	2.031	2.030	2.030	2.029	2.029
2.95	2.081	2.081	2.080	2.080	2.079	2.079
3.00	2.131	2.130	2.130	2.130	2.129	2.129
3.05	2.181	2.180	2.180	2.179	2.179	2.179
3.10	2.231	2.230	2.230	2.229	2.229	2.229
3.15	2.280	2.280	2.280	2.279	2.279	2.279
3.20	2.330	2.330	2.329	2.329	2.329	2.328
3.25	2.380	2.380	2.379	2.379	2.379	2.378
3.30	2.430	2.429	2.429	2.429	2.428	2.428
3.35	2.480	2.479	2.479	2.479	2.478	2.478
3.40	2.529	2.529	2.529	2.528	2.528	2.528
3.45	2.579	2.579	2.579	2.578	2.578	2.578
3.50	2.629	2.629	2.628	2.628	2.628	2.628

Percentile combination

b (mV)

k	100th-99.0th	100th-98.0th	100th-97.0th	100th-96.0th	100th-95.0th	100th-94.0th
2.50	-0.184	-0.230	-0.255	-0.274	-0.290	-0.302
2.55	-0.142	-0.190	-0.216	-0.235	-0.252	-0.264
2.60	-0.101	-0.151	-0.177	-0.197	-0.214	-0.227
2.65	-0.060	-0.111	-0.138	-0.158	-0.176	-0.189
2.70	-0.019	-0.071	-0.099	-0.120	-0.138	-0.152
2.75	0.023	-0.031	-0.060	-0.081	-0.100	-0.114
2.80	0.064	0.009	-0.021	-0.043	-0.062	-0.076
2.85	0.105	0.049	0.018	-0.005	-0.024	-0.039
2.90	0.146	0.088	0.057	0.034	0.014	-0.001
2.95	0.188	0.128	0.096	0.072	0.052	0.036
3.00	0.229	0.168	0.135	0.111	0.089	0.074
3.05	0.270	0.208	0.174	0.149	0.127	0.111
3.10	0.312	0.248	0.213	0.188	0.165	0.149
3.15	0.353	0.288	0.252	0.226	0.203	0.186
3.20	0.394	0.327	0.291	0.265	0.241	0.224
3.25	0.435	0.367	0.330	0.303	0.279	0.262
3.30	0.477	0.407	0.369	0.342	0.317	0.299
3.35	0.518	0.447	0.408	0.380	0.355	0.337
3.40	0.559	0.487	0.448	0.418	0.393	0.374
3.45	0.600	0.526	0.487	0.457	0.431	0.412
3.50	0.642	0.566	0.526	0.495	0.469	0.449

Percentile combination

Fig. 10. Parameters defining the conversion factor of Eq. (5) for different configurations of percentile combinations and 'k' values. The parameter 'a' (left) corresponds to the slope of the tendency line, while b (right) is the y-intercept. The parameters 'a' and 'b' providing the lowest RMSE in Fig. 11 are indicated by red ovals.

Fig. 10 contains the *a* and *b* parameters defining the conversion factor of Eq. (5) for all the 126 combinations obtained in this study, while Fig. 11 contains the RMSE values for the corresponding tendency line. As shown in Fig. 11, the optimal configuration that provide the lowest RMSE values is when *k* parameter is equal to 3.10 and the percentile combination is 100th-99th. The optimal configuration is obtained when the slope of the tendency line is 2.231 mV, parameter *a* in Fig. 10, and the y-intercept 0.312 mV, named as parameter *b* in Fig. 10. Therefore, the conversion factor that minimizes the RMSE is the following:

$$Conversion\,factor = \left(100^{th} - 99^{th}\right) \cdot 2.231 + 0.312(mV) \tag{6}$$

7.6. Conservative estimation of the RMS-QP relationship

In addition to the RMS-QP relationship obtained in the previous section, the use of a conservative estimation of that relationship is proposed, with the aim to provide a safety margin during the estimation of the QP values. The conservative estimation is based on the relationship described in Eq. (6), but overestimating the spectral values of the dataset used in the definition of the RMS-QP relationship. For obtaining this conservative estimation, the parameter *b* of the conversion factor, which is the y-intercept of the tendency line, has been adjusted to overestimate the spectral sample, maintaining the slope of the trendline, represented by the parameter *a*.

Table 3 contains the values to obtain a conservative conversion factor for overestimating different percentages of samples. To cover the 99 % of the samples, the parameter *b* is -3.078 mV (see Table 3), and the equation of the conservative conversion factor is the following:

$$Conservative\ conversion\ factor = \left(100^{th} - 99^{th}\right) \cdot 2.231 - 3.078\ (mV) \tag{7}$$

8. Approximated-QP and conservative-QP methods

The Approximated-QP (App-QP) and Conservative-QP (Cons-QP) methods are the techniques that have been developed taking advantage of the results obtained in this study about the relationship between RMS and QP values. Both methods are proposed with the aim of estimating QP values in the 150–500 kHz range. The App-QP method is based on the empirical relationship between the RMS and QP values in this frequency range, so it is useful for QP estimation, The Cons-QP method relies on the conservative estimation of the spectral samples, and therefore, it provides a conservative estimation of the QP spectra. Both techniques use the RMS values provided by the RM-A method, and then, they apply the outcomes of the statistical analysis described in the previous section to estimate the QP outputs from the RMS values.

The approach of these methods is different to the configuration of CISPR 16 receiver in Band B (0.15–30 MHz) [19], mainly in the procedure to calculate the QP values: the CISPR 16 receiver defines the performance of a QP detector, and the App-QP and Cons-QP methods are based on empirical relationships. Moreover, the RM-A method applies a non-overlapped rectangular window of 20 ms length, instead of the 0.5 ms length Gaussian window with a 90 % of overlap of the digital CISPR 16, which leads to a more accurate track of the quick impulsive disturbances by the CISPR 16 receiver. For this reason, a conservative estimation of the QP values is proposed in this study in order to cover those cases where the impulsive disturbances are hidden in the spectral calculation process of the RM-A method.

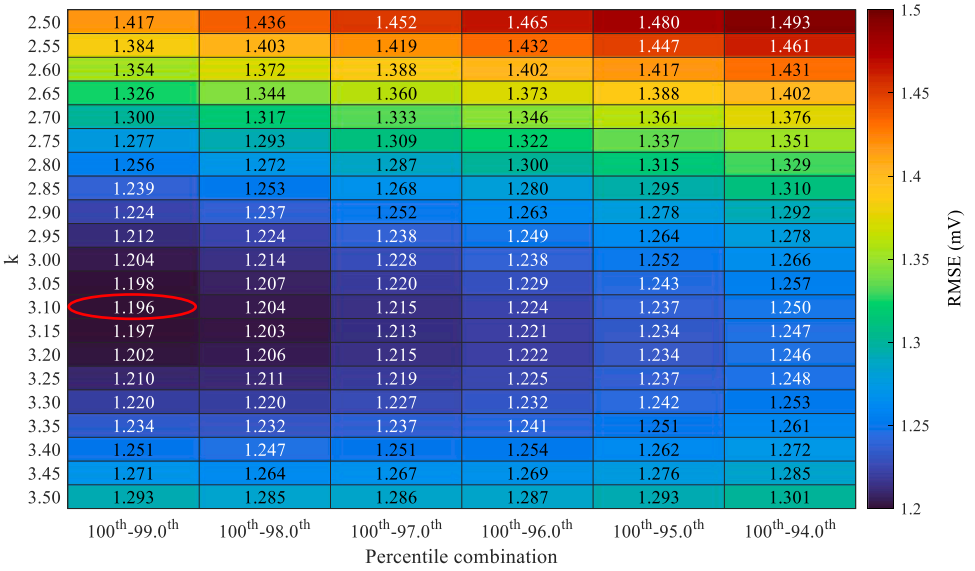

Fig. 11. Goodness of fit of the linear regression for the RMS-QP relationship. The parameter combination providing the lowest RMSE value is indicated with a red oval.

Table 3
Parameter of the conservative conversion factor for overestimating different percentages of the spectral samples.

Percentage of spectral samples overestimated	Conservative conversion factor		Percentage of spectral samples overestimated	Conservative conversion factor	
	a (mV)	b (mV)		a (mV)	b (mV)
85 %	2.231	−0.128	93 %	2.231	−0.848
86 %	2.231	−0.208	94 %	2.231	−0.988
87 %	2.231	−0.298	95 %	2.231	−1.198
88 %	2.231	−0.408	96 %	2.231	−1.358
89 %	2.231	−0.478	97 %	2.231	−1.518
90 %	2.231	−0.568	98 %	2.231	−1.728
91 %	2.231	−0.668	99 %	2.231	−3.078
92 %	2.231	−0.748	100 %	2.231	−23.318

This section describes the proposed methods, provides the accuracy results for the spectral outputs and evaluates their computational cost.

8.1. Description of the methods

Both App-QP and Cons-QP methods are defined in a two-step process, where the first stage is common for both techniques and the second stage relies on the conversion factors defined in this work (see Fig. 12). In the first stage, the spectral samples of both techniques are computed using the extension of the RM-A method to the 150–500 kHz band. Then, the outputs of the Fourier analysis, after been grouped to obtain a RBW of 9 kHz, are aggregated assessing the maximum amplitude of each frequency component in 200 ms and 3 s aggregation intervals. Finally, the peak spectral values and the instantaneous RMS values are used as input values to estimate the QP outputs, by applying the relationship obtained in this work.

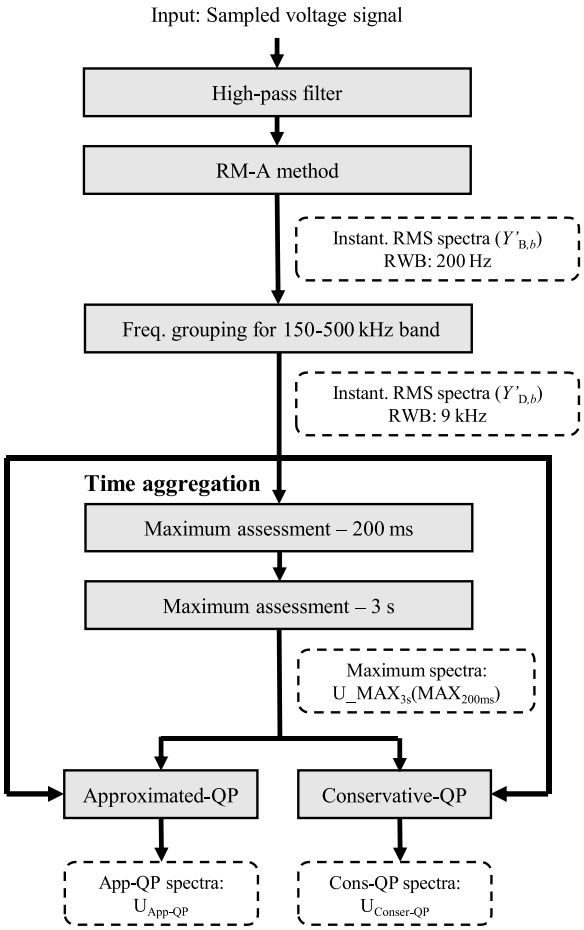

Fig. 12. Schematic overview of the Approximated-QP and Conservative-QP methods.

The App-QP takes the U_MAX$_{3s}$(MAX$_{200ms}$) and the 'conversion factor' to estimate the QP spectra in the 150–500 kHz band. The Eq. (8) shows the analytical expression to compute the App-QP values.

$$AppQP = k \cdot U\_MAX_{3s}(RMS_{200ms}) - Conversion\ factor =$$

$$3.10 \cdot U\_MAX_{3s}(RMS_{200ms}) - \left((100^{th} - 99^{th}) \cdot 2.231 + 0.312\right)(mV) \tag{8}$$

The Cons-QP method, represented in Eq. (9), uses the same variables as App-QP, but changing the value of the parameter b of the tendency line, to overestimate the QP spectral values in the 150–500 kHz band:

$$ConsQP = k \cdot U\_MAX_{3s}(RMS_{200ms}) - Conservative\ conversion\ factor =$$

$$3.10 \cdot U\_MAX_{3s}(RMS_{200ms}) - \left((100^{th} - 99^{th}) \cdot 2.231 - 3.078\right)\ (mV) \tag{9}$$

8.2. Accuracy analysis

The outputs of the methods proposed in this work are evaluated with respect the results obtained with a? digital implementation of CIPSR 16. This comparison is performed with a graphical representation of the outputs obtained with all methods, and also with a statistical analysis of the deviations in the results.

Regarding the graphical analysis, Fig. 13 and Fig. 14 represent the outputs obtained with the three methods used in this study for two measurements, one of them performed in an EVCS, and the other one at a POC of a LV distribution grid with PLC transmission. The results show that the App-QP method provides similar results to CISPR 16 in the 150–500 kHz band, while the Cons-QP method gives outputs of higher value than the results of the CISPR 16 method. These results clearly describe the aim of the Cons-QP method, which is to provide conservative QP outputs (in the 99 % of the cases being equal or higher, according to Table 3) with respect to the digital CISPR 16 receiver.

For the accuracy analysis, the 64 recordings of the 'validation' dataset were processed with the proposed techniques and compared to the outputs of the CISPR 16 method. The statistical analysis of deviations does not only evaluate the accuracy of the App-QP method with respect to the CISPR 16 receiver, but also how much the Cons-QP method overestimates the spectral values.

The evaluation of the App-QP method is performed by subtracting the results of the novel method and the digital CISPR 16 for all the frequency bins of the 64 recordings, and then calculating a set of statistics to characterize the deviations of the results. These metrics characterize the differences in absolute and relative values, e.g., the mean value of the absolute differences, the standard deviation of the absolute differences, the range of the 80 % and 90 % of the absolute differences (the difference 90th-10th and 95th-5th, respectively) and the median value of the relative differences. Additionally, the relevance of the absolute differences is that they represent the percentage of frequency bins whose absolute difference is below a percentage of the threshold level defined in this study. Table 4 contains the results of this comparison between App-QP and CISPR 16 outputs. The statistical analysis demonstrates that the differences of the results fall within a narrow range of few mV. Moreover, the dispersion of the values for percentages of 80 % and 90 % are in the same order of amplitude: the 80 % of the absolute differences are within the threshold value defined to remove the background noise, while the 90 % have differences below twice the threshold level. In addition, the median of the relative differences is close to 1.5 %.

With regard to the evaluation of the Cons-QP, the statistical analysis aims to quantify the overestimation of the spectral values. For this purpose, the selected metrics are the percentage of frequency bins overestimated by the Cons-QP and the overestimation level of the spectral samples by means of the median and the 90th percentile of the differences of the Cons-QP and CISPR 16 outputs. Table 5 shows the results of this analysis, proving that the Cons-QP method provides conservative QP values with respect to CISPR 16 in the 99.64 % of the cases for the validation dataset. Additionally, the metrics quantifying the absolute differences show that the differences are below 3.5 mV and 4.5 mV for the median and the 90th percentile, respectively.

The results showed in this section demonstrate that the App-QP method provides QP outputs comparable to the digital

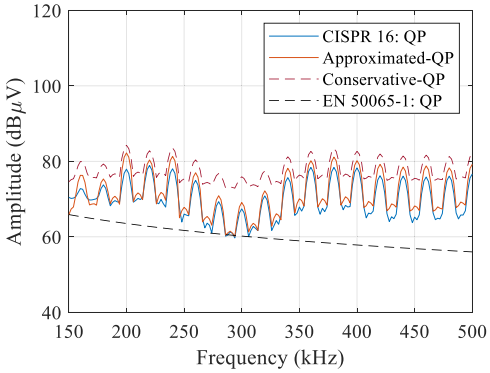

Fig. 13. Outputs from CISPR16, App-QP and Cons-QP methods for a measurement performed near an EVCS.

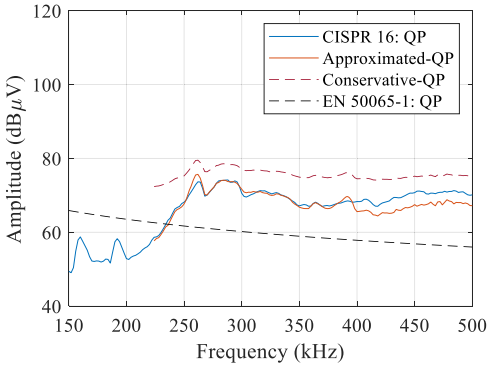

Fig. 14. Outputs from CISPR16, App-QP and Cons-QP methods for a measurement performed in LV distribution grid whit the presence of PLC transmissions.

Table 4
Comparison of App-QP and CISPR 16 outputs.

Absol. value of diff.				Relative diff.	Absolute diff. w.r.t. threshold	
Median	St. dev.	Range 80 %	Range 90 %	Median	Freq. bands with diff. $<$ thr.	Freq. bands with diff. $<$ 2 x thr.
0.002 mV	1.896 mV	1.126 mV	1.981 mV	1.417 %	81.01 %	90.83 %

Table 5
Comparison of Cons-QP and CISPR 16 outputs.

Percentage of samples overestimated	Absolute differences	
	Median	90th
99.64 %	3.402 mV	4.402 mV

implementation of CISPR 16 in the 150–500 kHz range. Furthermore, the Conservative-QP computes conservative QP outputs in the same frequency range with an overestimation of a few mV.

8.3. Performance of the methods

The computational cost and the memory requirements are key aspects when evaluating the measurement methods. This section addresses these aspects for the proposed methods comparing their performance to the CISPR 16. To estimate the computational complexity of the methods, the number of discrete Fourier transforms (DFTs) needed to compute the spectra of a 3-s long recording is calculated. As the processing time is also related to the computational cost of an algorithm, the elapsed real time and the CPU processing time of each method are calculated, which correspond to the real clock time needed for the execution of the algorithm and the time needed by all the cores of the CPU, respectively.

Table 6 contains the obtained requirements of the methods, where a clear difference is observed between the behavior of the CISPR 16 and the novel methods. CISPR 16 requires almost 60,000 DFTs to process a 3 s length measurement, while the new techniques only need 150 DFTs. This important difference on the number of DFTs, which is due to the time step of each method, has an impact on the rest of the metrics. App-QP and Cons-QP methods require 95 % less memory than the digital CISPR 16. Furthermore, the time needed to execute the novel methods is 92 % lower than for the standardized method, while the CPU processing time is 94 % lower.

The study on the performance of the methods clearly proves that the novel methods are less complex than the standardized CISPR 16. This aspect could be very important for the potential implementation of these techniques in inexpensive PQ meters.

9. Consistent measurement framework for the 9–500 kHz band

This paper has analyzed the existing measurement methods to identify the existing gaps and has proposed solutions to establish a consistent measurement framework in the entire 9–500 kHz range using the RM-A method as a basis. In this section, a novel measurement framework for the consistent characterization of the conducted emissions in the grid for the 9–500 kHz range is described (see Fig. 15). The measurement framework has been defined to ensure the consistency with standardized methods for frequencies below 9 kHz and to provide continuity of spectral results over the entire range. This framework has been designed to quantify the conducted emissions with the metrics defined in PQ standards (RMS and QP), to characterize the impulsive emissions separately, and to assess the emissions against the limits defined in standards, i.e., IEC 61000–2–2, EN 50065–1, CISPR 14–1, the CISPR 15 and the

Table 6
Computational requirements of App-QP, Cons-QP and CISPR 16 methods.

Method	Time step	Number of DFTs	Memory	Elapsed real time	CPU processing time
CISPR 16	0.05 ms	59,991	161.14 MB	25.14 s	114.58 s
App-QP	20 ms	150	8.41 MB	2.04 s	7.39 s
Cons-QP					

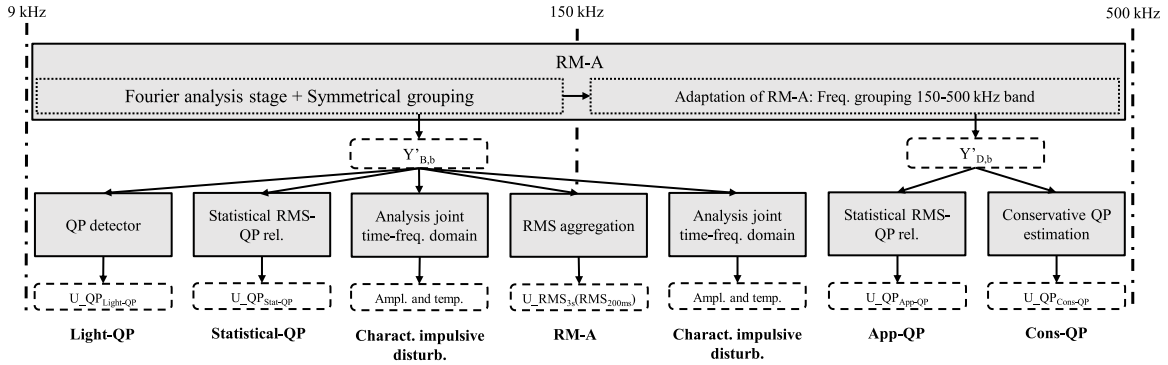

Fig. 15. Schematic overview of the proposed measurement framework.

CISPR 32.

As shown in Fig. 15, all the method use the instantaneous RMS outputs provided by the RM-A method [25] to compute the rest of the metrics. This method gives continuity with the techniques to obtain RMS values below 9 kHz and provides the same measurement configuration over the entire 9–500 kHz range, as well as continuity, and the possibility of relating metrics. Moreover, in this paper the feasibility of extending this method to the 150–500 kHz range has been analyzed.

Regarding the technique to quantify the impulsive disturbances [28], it detects and characterize the impulsive disturbances and discards the non-impulsive emissions applying a threshold. In this paper the suitability of the extension of this technique up to 500 kHz has been addressed.

In the process of defining this measurement framework, a set of RMS-QP relationships has been obtained for the 9–500 kHz range, with different configurations in the 9–150 kHz and 150–500 kHz ranges, but with the possibility of maintaining continuity of the

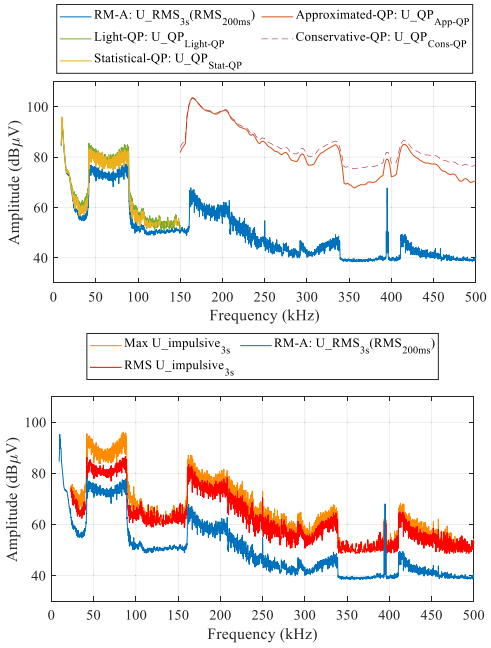

Fig. 16. Characterization of impulsive emissions in the LV distribution with the joint time-frequency domain proposed in this work for the 9–500 kHz: (up) results of RMS and peak values, (bottom) identification of number and duration of impulsive occurrences per 200Hz-frequency bin.

results. Specifically, the RMS-QP relationship for the 150–500 kHz range has been defined in this work.

The novel measurement framework contains the four methods for the calculation of QP values over the entire 9–500 kHz range. They are designed to respect the configuration required for the evaluation of conducted emissions against the limits established in the LV grid above and below 150 kHz. For the range 9–150 kHz, the published methods have been included (Light-QP [26] and Statistical-QP [27]) while for 150–500 kHz new methods have been defined in this paper (Approximated-QP and Conservative-QP), based on the RMS-QP relation proposed in this contribution.

An example of the application of the whole set of measurement methods is presented in this work. For this example, a measurement performed in the LV distribution grid, where PLC frames were transmitted, is used as input signal for all the methods. Fig. 16 contains the outputs of RM-A, Light-QP, Statistical-QP, Approximated-QP and Cons-QP for the amplitude characterization of the conducted emissions in the entire 9–150 kHz band. The methods measuring QP values follow the criteria defined in CISPR 16 below and above 150 kHz; therefore, each method provides values in a particular band with considerable differences in the configuration (see Fig. 16).

The RM-A provides RMS outputs in the entire band, and it is the basis for all the techniques that calculate QP outputs.

Fig. 16 contains the amplitude characterization of the impulsive disturbances present in the recording. Max U_impulsive$_{3s}$ is the maximum value of the impulsive disturbances, while *RMS* U_impulsive$_{3s}$ corresponds to the RMS spectra of those emissions over a 3 s measurement interval. Fig. 17 shows the temporal behavior of the impulsive disturbances characterized by means of the technique developed for the joint time-frequency domain. This analysis provides information about the number of events, the total and the mean duration of them, and the mean duration between impulsive disturbances in 3 s measurement intervals (see Fig. 17).

The measurement framework developed in this work provides a wide set of metrics not only to assess the compatibility limits defined in the grid in the 9–500 kHz range, but also to characterize the conducted emissions present in the grid. Moreover, these techniques provide additional information of the emissions not contemplated by the standardized methods, such as the analysis in the joint time-frequency domain.

10. Conclusions

This work aims to provide a consistent measurement framework for the 9–500 kHz range, being also consistent with the consolidated standard methods and metrics for frequencies below 9 kHz. The consistency of the measurement framework in the 9–500 kHz

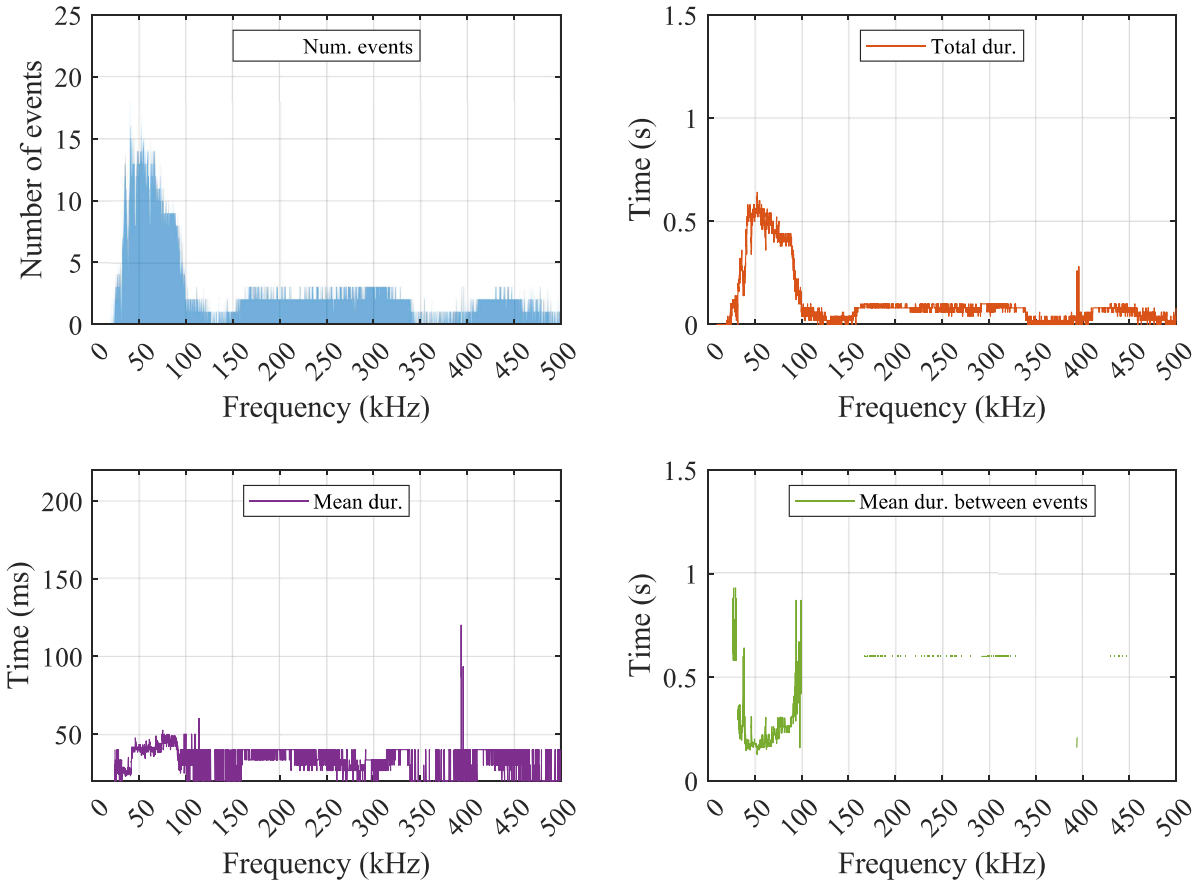

Fig. 17. Joint time-frequency characterization of impulsive disturbances recorded in the LV grid with the presence of PLC transmissions.

range facilitates the comprehensive comparison of emissions throughout the entire band, allowing for a thorough understanding of their significance. The novel framework presented in this paper proposes two novel and simple techniques to compute QP spectra in the 150–500 kHz range, extends some of the existing techniques up to 500 kHz, and summarizes the measurement methods that have been published recently.

The measurement framework takes the extension of the RM-A method up to 500 kHz as starting point to ensure the consistency in results in the entire 9–500 kHz range.

This paper demonstrates that the technique to characterize the impulsive disturbances in the joint time-frequency domain, which originally was defined for the 9–150 kHz band, is also valid for the entire 9–500 kHz range without requiring any modification.

The novel Approximated-QP and Conservative-QP methods for the measurement of the QP spectra in the 150–500 kHz band are presented in this contribution. These methods use the common basis defined in the measurement framework to compute the instantaneous RMS spectral of the measurements and take advantage of the relationship between RMS and QP proposed in this paper to estimate the QP values.

To conclude, this paper presents a novel measurement framework with six measurement techniques sharing a common initial stage based on Fourier analysis. Each technique provides tailored metrics to characterize conducted emissions as an optimized alternative to the fragmented standardized methods, ensuring consistency in results not only in the entire 9–500 kHz, but also with the PQ measurement framework defined below 9 kHz.

CRediT authorship contribution statement

Alexander Gallarreta: Conceptualization, Methodology, Software, Investigation, Writing – original draft. **Jon González-Ramos:** Investigation, Validation. **Stefano Lodetti:** Conceptualization, Methodology, Formal analysis, Writing – review & editing. **Peter Davis:** Conceptualization, Methodology. **Igor Fernández:** Formal analysis, Investigation. **David de la Vega:** Conceptualization, Methodology, Supervision, Writing – review & editing, Funding acquisition. **Itziar Angulo:** Investigation, Supervision. **Amaia Arrinda:** Supervision.

Declaration of competing interest

The authors declare that they have no known competing financial interests or personal relationships that could have appeared to influence the work reported in this paper.

Acknowledgements

The project 23IND06 Met4EVCS has received funding from the European Partnership on Metrology, co-financed from the European Union's Horizon Europe Research and Innovation Programme and by the Participating States. This work was funded in part by the Basque Government under the grants IT1436–22, PRE_2023_2_0037 and PRE_2023_2_0162. This work was financially supported in part by the Spanish Government under project THERESA, grant PID2021-124706OB-I00 funded by MICIU/AEI/10.13039/501100011033 and ERDF/EU 'A way of making Europe'. This work was funded in part by the UK Government's Department for Science, Innovation and Technology through the UK's National Measurement System.

Data availability

The data that has been used is confidential.

References

[1] Larsson EOA, Bollen MHJ, Wahlberg MG, Lundmark CM, Rönnberg SK. Measurements of high-frequency (2–150 kHz) distortion in low-voltage networks. IEEE Trans Power Deliv 2010;25. https://doi.org/10.1109/TPWRD.2010.2041371.

[2] Rönnberg SK, Bollen MHJ, Amaris H, Chang GW, Gu IYH, Kocewiak ŁH, Meyer J, Olofsson M, Ribeiro PF, Desmet J. On waveform distortion in the frequency range of 2 kHz–150 kHz—Review and research challenges. Electr Power Syst Res 2017;150. https://doi.org/10.1016/j.epsr.2017.04.032.

[3] Elfeki I, Jacques S, Aouichak I, Doligez T, Raingeaud Y, Bunetel JCLe. Characterization of narrowband noise and channel capacity for powerline communication in France. Energies 2018;11. https://doi.org/10.3390/en11113022.

[4] Kumar MS, Rani AJ. Reduction of conducted electromagnetic interference by using filters. Comput Electr Eng 2018;72. https://doi.org/10.1016/j.compeleceng.2018.09.002.

[5] Espín-Delgado A, Rönnberg S, Sudha Letha S, Bollen M. Diagnosis of supraharmonics-related problems based on the effects on electrical equipment. Electr Power Syst Res 2021;195. https://doi.org/10.1016/j.epsr.2021.107179.

[6] Bollen MHJ, Das R, Djokic S, Ciufo P, Meyer J, Rönnberg SK, Zavodam F. Power quality concerns in implementing smart distribution-grid applications. IEEE Trans Smart Grid 2017;8. https://doi.org/10.1109/TSG.2016.2596788.

[7] Dkhili N, Eynard J, Thil S, Grieu S. A survey of modelling and smart management tools for power grids with prolific distributed generation. Sustain Energy Grids Netw 2020;21. https://doi.org/10.1016/j.segan.2019.100284.

[8] Rajkumar S, Balasubramanian R, Kathirvelu P. A comprehensive review on supraharmonics—The next big power quality concern. Smart Grids Energy 2024;9. https://doi.org/10.1007/s40866-024-00195-4.

[9] Shrestha D, Mestre X, Payaró M. On channel estimation for power line communication systems in the presence of impulsive noise. Comput Electr Eng 2018;72. https://doi.org/10.1016/j.compeleceng.2018.10.006.

[10] Pereira SC, Casella IRS, Capovilla CE, Sguarezi Filho AJ, Costa FF. Power line communication technology based on morphological filtering for machine-to-machine applications. Comput Electr Eng 2021;93. https://doi.org/10.1016/j.compeleceng.2021.107254.

[11] Khokhlov V, Meyer J, Grevener A, Busatto T, Rönnberg S. Comparison of measurement methods for the frequency range 2–150 kHz (Supraharmonics) based on the present Standards framework. IEEE Access 2020;8. https://doi.org/10.1109/ACCESS.2020.2987996.
[12] Electromagnetic compatibility (EMC) - environment - compatibility levels for low-frequency conducted disturbances and signalling in public low-voltage power supply systems, IEC 61000-2-2:2002+A2:2019 ed. 2.2, 2002.
[13] CENELEC, "Signalling on low-voltage electrical installations in the frequency range 3 kHz to 148,5 kHz – Part 1: general requierements, frequency bands and electromagnetic disturbances", EN 50065-1, 2011.
[14] International Electrotechnical Commission. Electromagnetic compatibility - requirements for household appliances, electric tools and similar apparatus - part 1: emission. CISPR 2020;14-1:2020.
[15] International Electrotechnical Commission. Limits and methods of measurement of radio disturbance characteristics of electrical lighting and similar equipment. CISPR 2018;15:2018.
[16] International Electrotechnical Commission. Electromagnetic compatibility of multimedia equipment - emission requirements. CISPR 2015;32. +AMD1:2019, 2019.
[17] International Electrotechnical Commission, "Electromagnetic compatibility (EMC) - part 4-7: testing and measurement techniques - general guide on harmonics and interharmonics measurements and instrumentation, for power supply systems and equipment connected thereto", doc. IEC 61000-4-7:2002+AMD1:2008.
[18] International Electrotechnical Commission, "Electromagnetic compatibility (EMC) - part 4-30: testing and measurement techniques - power quality measurement methods", doc. IEC 61000-4-30 Ed.3, 2015.
[19] International Electrotechnical Commission. Specification for radio disturbance and immunity measuring apparatus and methods - part 1-1: radio disturbance and immunity measuring apparatus - measuring apparatus. CISPR 2019;2019. 16-1-1.
[20] Azpurua MA, Pous M, Oliva JA, Pinter B, Hudlicka M, Silva F. Waveform approach for assessing conformity of CISPR 16-1-1 measuring receivers. IEEE Trans Instrum Meas 2018;67. https://doi.org/10.1109/TIM.2018.2794941.
[21] Mendes TM, Duque CA, Silva LRM, Ferreira DD, Meyer J. Supraharmonic analysis by filter bank and compressive sensing. Electr Power Syst Res 2019;169. https://doi.org/10.1016/j.epsr.2018.12.016.
[22] Mendes TM, Ferreira DD, Silva LRM, Khosravy M, Meyer J, Duque CA. Supraharmonic estimation by polyphase DFT filter bank. Comput Electr Eng 2021;92. https://doi.org/10.1016/j.compeleceng.2021.107202.
[23] Lodetti S, Bruna J, Melero JJ, Khokhlov V, Meyer J. A robust wavelet-based hybrid method for the simultaneous measurement of harmonic and supraharmonic distortion. IEEE Trans Instrum Meas 2020;69. https://doi.org/10.1109/TIM.2020.2981987.
[24] Li K, Zhao W, Li S, Huang S. Supraharmonics measurement based on colored noise suppressed matrix pencil method. IEEE Access 2023;11. https://doi.org/10.1109/ACCESS.2023.3311258.
[25] Gallarreta A, Fernández I, Ritzmann D, Lodetti S, Khokhlov V, Wright P, Meyer J, de la Vega D. Adaptation of the IEC 61000-4-7 measurement method to CISPR band A (9-150 kHz). In: 2022 IEEE 12th International Workshop on Applied Measurements for Power Systems; 2022. https://doi.org/10.1109/AMPS55790.2022.9978818.
[26] Gallarreta A, Fernández I, Ritzmann D, Lodetti S, Khokhlov V, Wright P, Meyer J, de la Vega D. A light measurement method for 9-150 kHz disturbances in power grids comparable to CISPR Quasi-Peak. IEEE Trans Instrum Meas 2022. https://doi.org/10.1109/TIM.2022.3195255.
[27] Gallarreta A, Fernández I, Ritzmann D, Lodetti S, Khokhlov V, de la Vega D, Wright P, Meyer J. Statistical relationship between RMS and QP spectra of voltage measurements in the 9–150 kHz range. Electr Power Syst Res 2023;218. https://doi.org/10.1016/j.epsr.2023.109213.
[28] Gallarreta A, Fernández I, González-Ramos J, de la Vega D, Angulo I, Arrinda A. Technique for the comprehensive characterization of supraharmonic disturbances (9–150 kHz) in the joint time-frequency domain",Sustainable Energy. Grids Netw 2023;36. https://doi.org/10.1016/j.segan.2023.101181.
[29] Gallarreta A, Lodetti S, Davis P, González–Ramos J, Fernández I, de la Vega D, Angulo I, Arrinda A. Analysis of requirements for a measurement method to assess conducted disturbances in the 2–500 kHz band. In: 2023 IEEE 13th International Workshop on Applied Measurements for Power Systems (AMPS); 2023. https://doi.org/10.1109/AMPS59207.2023.10297233.
[30] Fernández I, Alberro M, Montalbán J, Arrinda A, Angulo I, de la Vega D. A new voltage probe with improved performance at the 10 kHz–500 kHz frequency range for field measurements in LV networks. Measurement 2019;145. https://doi.org/10.1016/j.measurement.2019.05.106.